

気流に垂直な平面と凹および凸曲面の極超音速衝撃波 形状に関する研究

ヴァシシュタ アシシュ (東大院), 渡邊 保真 (東大工学系), 鈴木 宏二郎 (東大新領域)

Study of Shock Shape in front of Concave, Convex and Flat Arc in Hypersonic Flow

by

Ashish VASHISHTHA¹⁾, Yasumasa WATANABE²⁾ and Kojiro SUZUKI³⁾

¹⁾ Doctoral Student, Department of Advanced Energy, Graduate School of Frontier Sciences, The University of Tokyo

²⁾ Assistant Professor, Department of Aeronautics & Astronautics, Graduate School of Engineering, The University of Tokyo

³⁾ Professor, Department of Advanced Energy, Graduate School of Frontier Sciences, The University of Tokyo

ABSTRACT

In this study, the bow-shock shape has been studied in front of finite length semi-circular convex, concave cylindrical arc and flat plate at hypersonic Mach number 7. The experiments were carried out in hypersonic wind tunnel for drag coefficient measurement and shock visualization using Schlieren method. Further, numerical simulations were performed for the finite length concave, convex and flat plate geometries by solving three-dimensional Navier-Stokes equations for wind tunnel test-section conditions. The effect of curvature on shock envelope and drag coefficient for these three geometries is studied. It is also observed that the same reference area of concave arc can produce instabilities in shock wave, which can lead to starting problem of tunnel. Hence, the Schlieren images were captured using high-speed camera with 5000 fps. The different patterns of shock instabilities have been observed in case of concave shape cylindrical arc. Among the different instability patterns, particle induced instability pattern has been studied by numerical simulation by using static particle located upstream of concave geometry in hypersonic flow simulation.

1. Introduction

The fore-body shape of a moving object is an important parameter, which influence the flow field around it and the drag force on the body. In hypersonic flows, the total drag on a blunt body can be classified into three main components as wave drag, base drag and skin-friction drag. The fore-body shape influences the wave drag and heat transfer in hypersonic flow, because of the shock strength and shape of shock wave. To reduce the wave drag and to decrease the heat load in hypersonic flows at the fore-body, many active and passive controls has been studied. But, the main aim of all techniques is to modify the shape of the bow shock in front of fore-body.

The breathing blunt nose (BBN) concept as a passive technique in hypersonic flows has been demonstrated by Imamura et al. [1], which enables to bring bow shock closer to blunt nose by taking the flow through the nose and this concept was further investigated for lifting body configuration by Khurana et al. [2]. Similarly, the effect of forward-facing cavity on aerodynamic coefficients and heat transfer was investigated by Saravanan et al. [3].

To push the bow shock away from the lifting body configurations, the application of aero-spikes at Mach number 7 hypersonic flow, has been studied by Khurana et al. [4]. The effect of supersonic counter-flow jet at the bow shock in front of blunt body has been studied in hypersonic flows as an active technique by Bala et al. [5], which works as virtual aero-spike. Similarly, Laser induced aero-spike was also used as active technique for drag reduction [6]. The passive techniques have been advantageous over active techniques, as passive techniques do not require extra energy source. The aim of passive or active techniques is to modify the bow shock shape in front of the fore-body by bringing it closer to the blunt body or by moving it away from the blunt body.

In low subsonic speed, the effect of concave, convex arc and flat plate shapes on flow field around the geometries have been studied by Sharma et al. [7], and it is found that flow field around the body can be manipulated by these geometrical shapes as location of stagnation pressure point as well as shape of twin vortices behind the body changes because of curvature. The effect of concave shaped geometry has been studied for parachute application in supersonic flows by Keishi et al. [8].

The main aim of this study is to study the effect of different geometric shapes, convex cylindrical arc (CVA), flat plate (FP) and concave cylindrical arc (CCA) on the shock shapes to understand the flow field around these cylindrical arcs and flat

plate at hypersonic Mach number 7. The three geometries have been tested at Mach number 7 hypersonic flow experimentally and three-dimensional numerical simulation was carried out for the same standard test-section conditions. The drag coefficients for these geometries are compared experimentally and numerically. The flow visualization of shock waves is also carried out by using Schlieren method and compared with the numerical simulation. The flow visualization by using high-speed camera, with 5000 fps, reveals the shock instability for all shapes of geometry. The shock instability in the case of concave arc is more frequent than in case of convex arc or flat plate. Mizukaki et al. [9] has studied the instability characteristics of shock waves before the hemi-spherical shell in supersonic flow and found that the shock wave oscillations appear above Mach 3. It was assumed by Mizukaki et al. [9] that density disturbances in the cavity might have caused the shock oscillation at supersonic speeds. As in the present study, the instabilities have been seen with convex shape arc and flat plate also, it is understood that there might be several reasons of shock instabilities e.g. high-speed flow perturbations, structural oscillation of object in high-speed, instability of the vortices in the stagnation zone of the geometry (aerodynamic instability) or high-speed particle impact at the shock wave. From many reasons of instability it is required to identify the different pattern of instability. In this study one pattern of instability has been presented, which is assumed to be because of particle impact. A static particle at certain upstream location is assumed and shock interactions were computed numerically and compared with unstable shock shape visualized experimentally.

2. Experimental Method

2.1. Wind Tunnel

The experiments were carried out at Kashiwa Hypersonic and High-Temperature Wind Tunnel [10], at Graduate School of Frontier Sciences, The University of Tokyo. Fig.1 shows the perspective view of wind tunnel facility.

The wind-tunnel test-section is designed for uniform core of 120 mm diameter Mach number 7 flow-field with maximum stagnation pressure as 950 kPa and maximum stagnation temperature as 1000 K. The specifications of hypersonic wind tunnel are listed in Table 1. The force measurement was done by six-component force balance system. The time averaged drag force has been calculated in this experiment. Although, the stagnation pressure was remained almost constant as 957 kPa, the

stagnation temperature varies from 500 K to 600 K, during the run time for the three blows of wind tunnel.

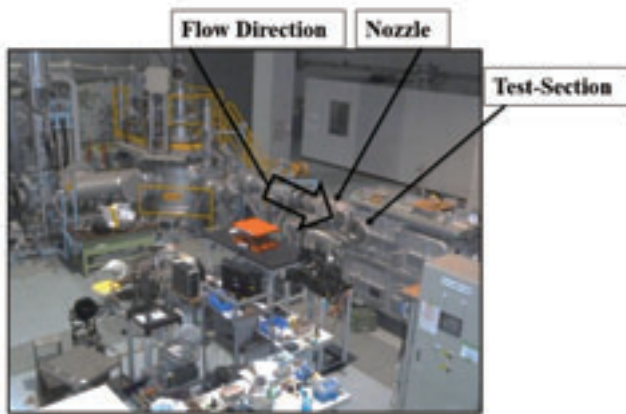


Figure 1: Kashiwa Hypersonic and High Temperature Wind Tunnel

Table1: Hypersonic Wind Tunnel Specifications [10]

Mach Number	7.0
Unit Reynolds Number	1.0×10^4 (1/cm)
Stagnation Pressure	Maximum 0.950 MPa
Stagnation Temperature	Maximum 1000 K
Mass Flow Rate	Maximum 0.39 kg/sec.
Nozzle Exit	200 mm diameter
Run Time	60 sec.

2.2. Experimental Model

In this study, three shapes of geometries have been used as shown in isometric view in Fig. 2. Initially, the convex, concave cylindrical arc and flat plate were fabricated with the same projection area of 30 x 30 mm². During the experiment it is observed that concave arc of same projection area as other two geometries can lead to the starting problem of tunnel. In most cases, the starting problem of wind tunnel is due to blockage caused by test model. In case of concave shape cylindrical arc, which has more blunt-nosed portion compared with the other two, it may cause higher effective blockage area which makes the blockage constraint severe. Hence, it was required to reduce the size of concave shaped model. Further, the concave cylindrical arc has been fabricated for 20 x 20 mm² projection area. All the experimental results have been compared as non-dimensional parameters for the geometries used in the experiments.

The two-dimensional projection views of experimental models are shown in Fig. 3. The experimental models were attached to force balance with ϕ 6 mm screw as connecting rod in the test-section with zero angle of attack.

2.3. Flow Visualization

The flow visualization was conducted using twin mirror Schlieren system with sodium lamp as light source. A high-speed video camera, Phantom Miro eX4 was used for capturing the Schlieren video and further frames test-section extracted for the same. The frame size captured in test section was 320 x 240 pixels around the model. The frame rate was used as 5000 fps with exposure time of 197.5 μ sec. The camera was manually triggered after the flow was established in test-section to capture the shock wave in the hypersonic flow. Due to internal memory capacity limit, the video was captured for 3.6824 seconds. Further, the instabilities in the flow field have been observed with high-speed camera for flow around concave cylindrical arc as well as for flat plate and convex arc. The X-direction is assumed in the flow direction, while Y and Z- directions were assumed as shown in Fig. 2 for three geometries. The flow visualization was done in XY plane to visualize the shock waves in the plane of curvature of concave and convex arcs and XY plane of flat plate.

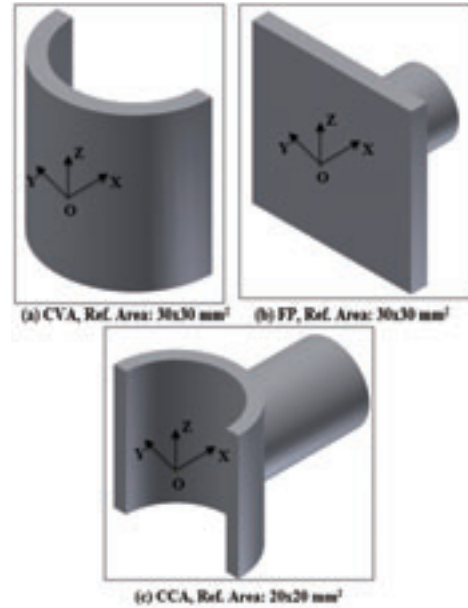


Figure 2: Isometric Views of (a) Convex Cylindrical Arc, (b) Flat Plate and (c) Concave Cylindrical Arc.

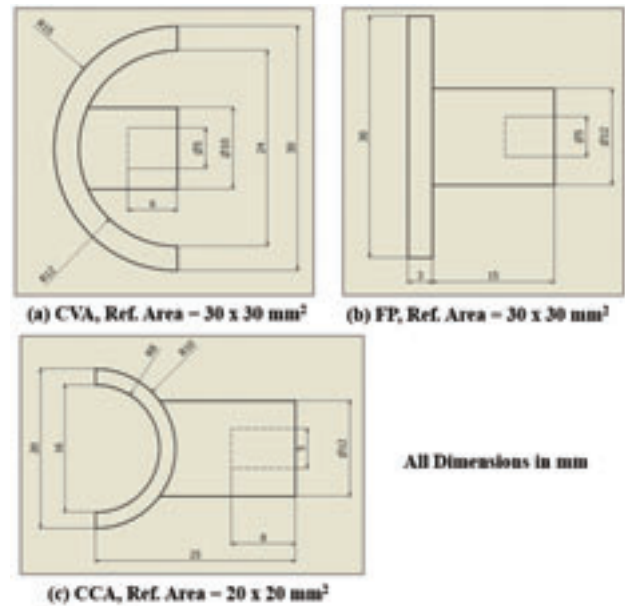


Figure 3: 2-D Views with of (a) Convex Cylindrical Arc, (b) Flat Plate and (c) Concave Cylindrical Arc

3. Numerical Method

3.1. Computational Domain

The numerical simulations were carried out for qualitative visualization of shock shape in three dimensions as well as to compare the drag coefficient for different geometries. Further, the computation was carried out to visualize the particle-induced instability pattern captured during experiment only for concave semi-circular shape finite length cylinder.

The two dimensional structured grid was generated for concave, convex arc and flat plate which is shown in Fig. 4. It is required to highly refine the domain near the arc and flat plate zone to capture the shock wave. The whole domain was filled with grid points, while during computation, the boundary conditions are given as zero velocity inside the geometry and no-slip boundary conditions at the surfaces. The grid points in three dimensions are shown in Fig. 5 for all the three geometries.

All the three geometries were considered as concave arc, convex arc as semicircle with diameter 20 mm and thickness of 2 mm, and flat plate with 20 mm reference length with 2 mm

thickness. The height of the cylindrical arcs and flat plate was considered as 20 mm. The main aim of this study is to qualitatively compare the shock shapes for these three geometries and compare the drag coefficient. Hence, the grid is much refined at the upstream of the geometry and it is coarser near the center of base, which can reduce the computation time also.

Further the flow instability has been investigated by extending the domain upstream and introducing a static particle in form of solid cell of size 0.2 mm at upstream location (-20,0,0) with no-slip boundary condition.

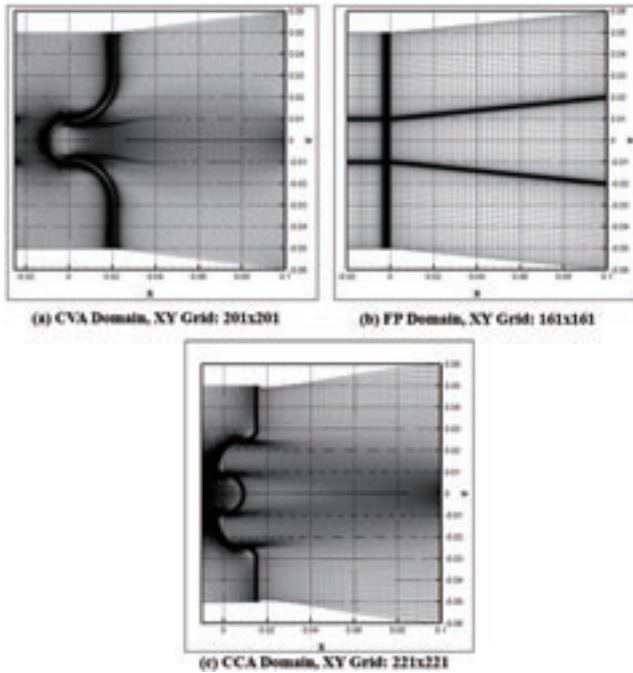


Figure 4: 2D Structured Grid for Convex, Flat Plate and Concave Cylindrical Arc.

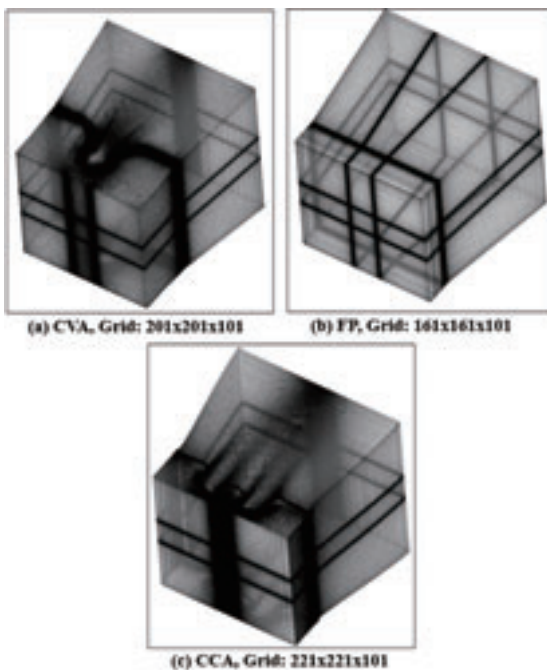


Figure 5: 3D domain for Convex, Flat Plate and Concave Cylindrical Arc.

3.2. Numerical Scheme

The numerical analysis was conducted using three-dimensional Navier-Stokes equations for unsteady laminar

compressible flows. As a spatial discretization method, second-order Yee's Symmetric TVD Scheme [11] is employed and the viscous terms are evaluated with second order central differential scheme. Third order TVD Runge-Kutta method [12] was employed as a time integration method. The boundary condition at the inlet surface is used as hypersonic wind tunnel test-section conditions, Mach no. 7, stagnation pressure as 950 kPa and stagnation temperature as 600 K. The boundary condition at the side boundaries is used as free-stream, while supersonic outlet for the outflow surface. The wall boundary is assumed to be a no-slip, and with isothermal constant temperature, as 300 K.

3.3 Grid Independence Test

The grid independence test was performed for three grid sizes for concave arc (CCA), 173x173x101 (grid 1), 221x221x101 (grid 2) and 261x261x101 (grid 3), respectively. The drag coefficient was calculated for these three grids with solution time of 100000 iterations. The calculated drag coefficient is shown in Fig. 6. The difference in drag coefficient is almost same as between grid 1 and grid 2 as the same between grid 2 and grid 3. Hence grid 2 (221x221x101) was used for numerical study for concave cylindrical arc, to reduce computation time. Similarly, for convex cylindrical arc and for flat plate grid sizes of 201x201x101 and 161x161x101 were chosen, respectively.

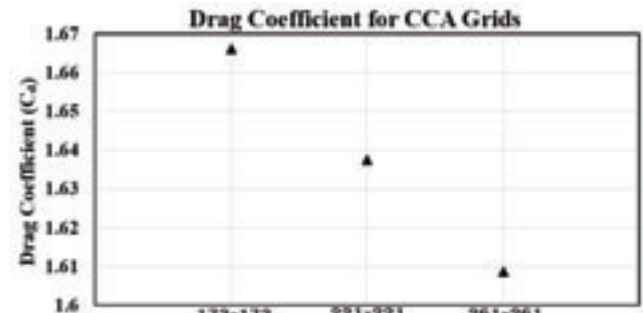


Figure 6: Drag Coefficient for three different grid sizes (in X-Y) for CCA

4. Results

It is to note that during the experiments, the reference area for concave cylindrical arc (CCA) is $20 \times 20 \text{ mm}^2$, while reference area for convex, cylindrical arc (CVA) and flat plate (FP) is $30 \times 30 \text{ mm}^2$ and for numerical simulations all the three geometries were used as $20 \times 20 \text{ mm}^2$ reference area.

4.1. Drag Coefficient

The time averaged drag force is calculated by the measured drag force for the geometric models, during steady operation of wind tunnel test-section. It is further non-dimensionalized by free-stream dynamic pressure and projection area to calculate the drag coefficient (C_d). In the experimental model, the model is connected to the balance with the connecting rod. The experimental and numerical drag force coefficients are plotted w.r.t. three geometries in Fig. 7. It is observed that the experimental drag coefficient is minimum for convex geometry (CVA) and it increases for flat plate (FP) and further increases for concave geometry (CCA). It is expected, as streamlined convex geometry should have least drag coefficient than flat plate and concave geometry. However, between flat plate and concave geometry, it is higher for concave geometry because of cavity like trapped higher stagnation area than flat plate.

The numerical drag coefficient was calculated for steady state solution and there is no connecting rod in numerical simulations. It is observed that numerical drag coefficient is lesser than experimental drag coefficient for all the geometries. It can be explained as presence of connecting rod, the viscous drag of connecting rod can contribute in experimental drag coefficient,

while its presence can also reduce or elongate the wake area, depends on the wake of geometry, hence it can also contribute towards reducing base drag. Hence, the numerical drag coefficient is lesser but comparable for experimental drag coefficient of convex cylindrical arc and flat plate. Further, the difference between concave arc of 20 mm reference length and convex arc of 30 mm reference length is more comparable area behind the base is occupied by connecting rod, which may lead to higher experimental drag coefficient than numerical drag coefficient for concave geometry.

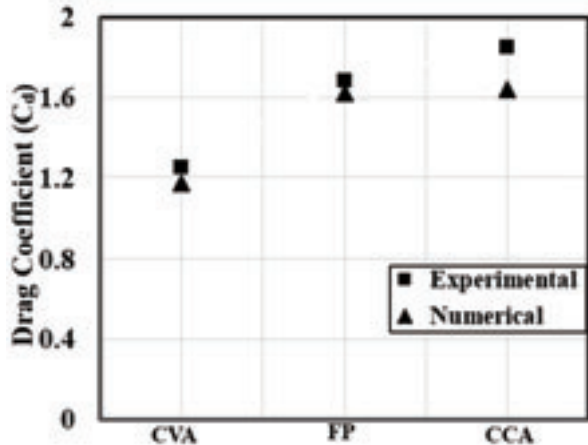


Figure 7: Experimental and Numerical Drag Coefficient w.r.t. Geometries

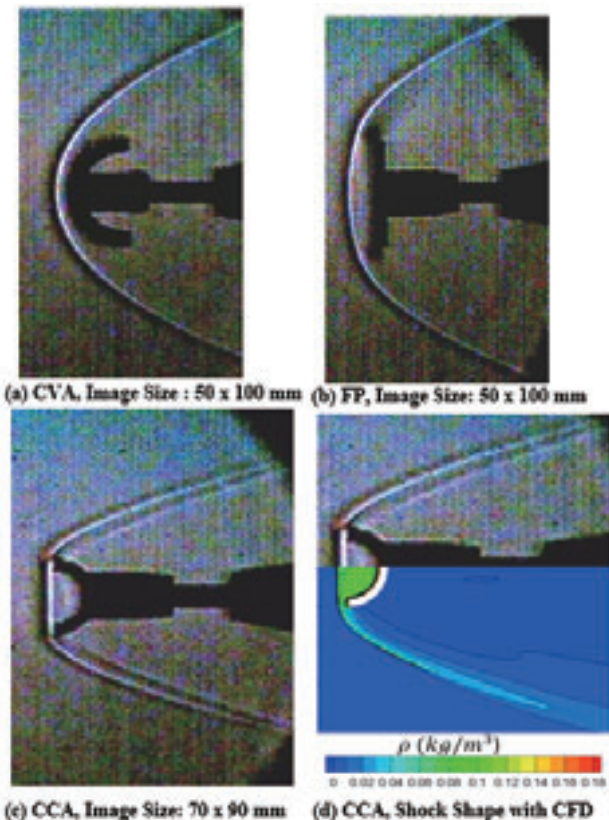


Figure 8: Schlieren images for (a) CVA, (b) FP and (c) CCA from experiments, (d) Comparison between numerical and experimental Shock Shape for CCA

4.2 Visualization of shock waves:

The shock waves were visualized using twin mirror Schlieren system. The captured Schlieren images with the actual sizes have been shown in Fig.8a, 8b and 8c. The left edge of the image is at 10 mm upstream distance from center point of convex cylindrical arc and flat plate, while for concave shaped arc, from its edges. It

can be seen from Fig. 8a and 8b that by changing the curvature from convex to flat, the central area of shock wave moves upstream and become bigger for flat plate as well as there is slight change in angle of the downstream shock for flat plate as compare to convex arc. The normal shock zone is bigger for flat plate than compare to convex geometry. This structure of shock wave in front of flat plate leads to higher drag coefficient.

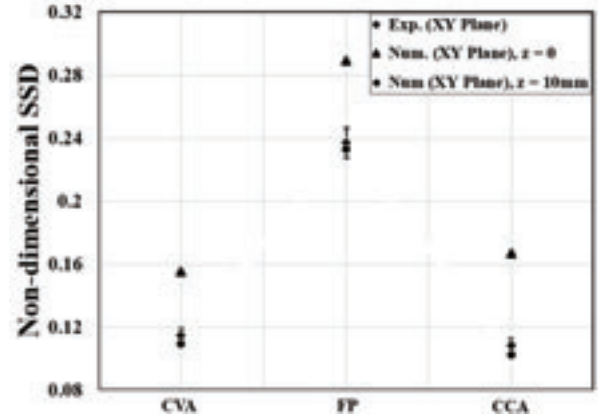


Figure 9: Non-dimensional Shock Stand-off distance for CVA, FP and CCA, experimental value and numerical values for XY plane at z =0 and z = 10 mm.

Further, by comparing the shock shape from Fig. 8a, 8b and 8c, it is clear that the shock envelop for CCA has been shrunk and elongated as the angle of the downstream shock with the horizontal line has been reduced, while the normal shock area extends and covers the whole area in front of concave arc geometry. The comparison between CCA Schlieren shock and density contour has been qualitatively done in Fig. 8d., while the quantitative force values may determine the higher drag coefficient in experimental results of concave shape than compare to numerical drag coefficient.

The shock stand-off distance has been calculated for convex geometry and flat plate as a distance from stagnation point and further non-dimensionalized by reference length, while for concave geometry, it is calculated from the edge of concave arc to the extent of shock wave at the center of arc. It is also non-dimensionalized with reference length of arc and flat plate. The non-dimensional shock stand-off distance (SSD) has been plotted for the geometrical shapes in Fig. 9. The numerical shock stand-off distance has been calculated for XY plane at the center location and at the edge (z= 10 mm) of the geometries. It is observed that the highest shock stand-off distance is for flat plate (FP), while for concave shape, the shock becomes a little closer to the geometry. As the experimental shock visualization is conducted by Schlieren system, which captured the light rays passing through the three-dimensional shock envelop. It can be seen that experimental shock stand-off distance lies between central shock stand-off distance the shock extent at the edge for concave, convex cylindrical arc and flat plate. Although, all the experimental non-dimensionalized shock stand-off distances closely match with the shock extent near the edge for numerical shock stand-off distance, It can be observed there is significant gap between numerical results of shock stand-off distance between center plane and z = 10 mm plane. This gap is minimum for convex arc, while it increases for flat plate and concave arc. This is because the shock angle at the edge changes more for concave in comparison to flat plate or convex shape arc.

The density contours has been shown in Fig. 10 as numerical results for CCA, FP and CVA. The contours have been plotted in XY and XZ central plane. In Fig.10, from the XY plane contours, it is quite visible as the minimum shock stand-off distance is for concave geometry, while the flat plate pushes the shock wave more upstream direction than concave or convex arcs. By

comparing the XZ plane density contours, it is observed that minimum shock stand-off distance is for convex shape, while concave shape shows more area of stagnation because of cavity in front of concave shape. While from the edges of concave arc, the shock stand-off distance remains lesser than convex arc or flat plate.

From the above observations, it is quite understood that, the shock stand-off distance is highest for flat plate, as well as extent of stagnation zone in front of flat plate while for concave shape the shock stand-off distance is lowest among three geometries because the cavity in front of concave arc can accommodate the stagnation zone. Further, the drag coefficient is highest for concave shape cylindrical arc as compare to flat plate and convex shape cylindrical arc.

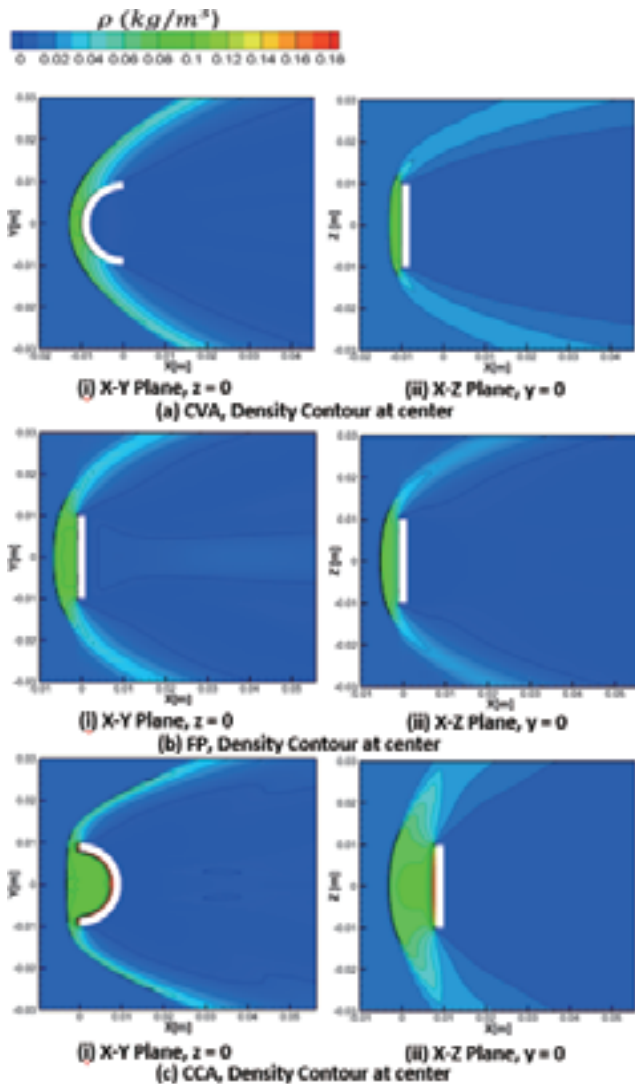


Figure 10: Density Contour for (a) CVA, (b) FP and (c) CCA from experiments, in XY and XZ planes.

4.3 Instability of shock wave shape

During the experiment of 30 mm reference length concave arc, it was observed that same reference area as flat plate and convex shaped cylindrical arc, the concave shape cylindrical arc, can produce unstable flow in the wind tunnel test-section which can lead to starting problem of tunnel. Hence, it was decided to reduce the size of concave arc to 20 mm reference length as well as to capture Schlieren images by using high-speed camera. By using 5000 fps camera, it is found that there are many pattern of instabilities in the case of concave shaped cylindrical arc. Although, small amplitude shock oscillations were also observed in case of convex shaped arc and flat plate, with very less number

of small shock instability as compare to concave shaped cylindrical arc, where the shock wave shape has completely modified.

There can be many reasons for shock instability for concave cylindrical arc as high perturbations in flow field, structural oscillation of concave edges, and instability of trapped vortices in cavity area which can leads to weakening the shock (aerodynamic instability) or impact of small particles from the stagnation chamber to the shock wave.

In the present study, the instability pattern due to particle impact has been observed and simulated by numerical simulation. Here, in numerical simulation, the motion of particle has been neglected and one particle is assumed as static at certain location. The particular location of particle can be calculated by Schlieren image of instability pattern. Although, steady state numerical simulation cannot address the complete phenomenon of particle induced instability, but this numerical simulation can help to distinguish the instability pattern induced by particle and its extent in three dimension.

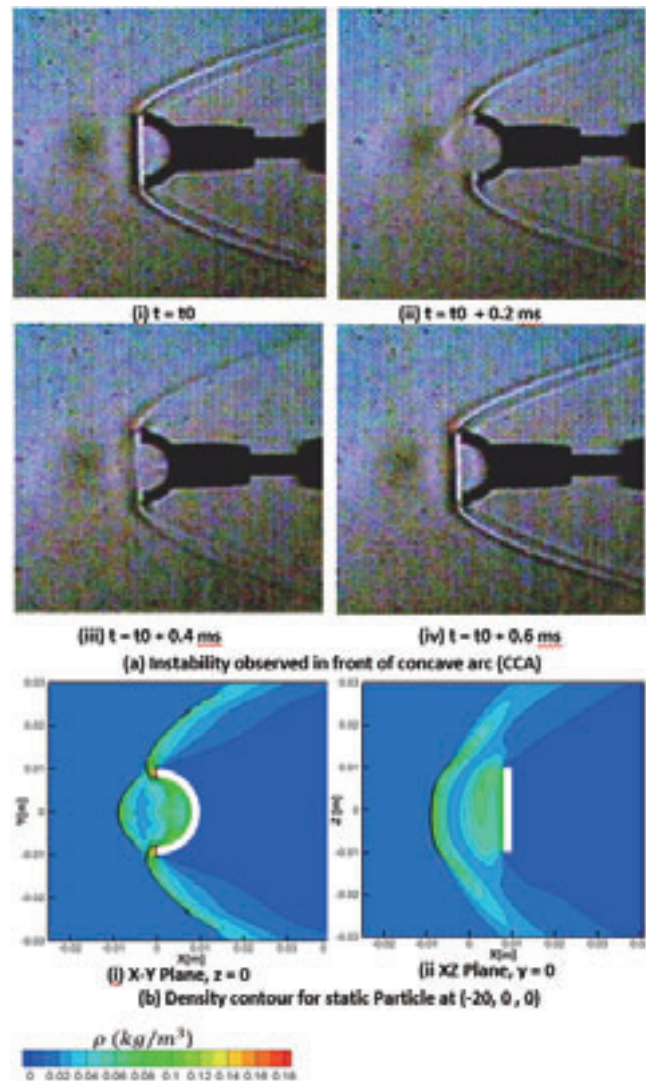


Figure 11: Schlieren image of one instability and corresponding CFD results for instability due to particle.

Figure 11a, shows the experimentally observed instability. In Fig. 11a the four frames are sequential frames with the time interval of 0.2 msec. The instability appears at time $t_0 + 0.2$ msec and disrupt the center of the shock wave and the central shock has been moved to upstream. This instability has weakened the shock wave in next frame at $t_0 + 0.4$ msec. After 0.6 msec, the shock has

been positioned at the same location. To further understand the flow physics during the instability it is required to use higher frame rate camera or use numerical simulation.

In the numerical simulation, one cell of the size 0.2 mm at the location of (-20, 0, 0) mm has been given as zero velocity and no-slip boundary condition at its wall to see the effect of its shock interaction with main shock and shock pattern through numerical simulation.

In Fig. 11b, the steady state density contour is plotted for XY plane as well as for XZ plane. It can be seen that the experimental shock pattern of Fig 11a (ii), can be compared with numerical result in Fig 11b (i). The shock generated by the particle can hit at the edges of the concave arc and produce the similar pattern as seen in experiment. From XZ density contour, it can be further seen that the shock generated by particle, does not interact with the main shock near the body as the main shock is already more inclined near the edges for without particle case.

5. Conclusion

In this study, the three different geometry shapes concave, convex and flat plate have been tested in form of finite length semi-circular cylindrical arcs in hypersonic wind tunnel. The first observation was made that the same size and projection area geometry of concave shape can produce high instabilities, which can lead to starting problem for tunnel. Further, the effect of different geometrical shapes on total drag and shock stand-off distance has been studied. It is found that the concave shape geometry is subjected to highest drag among three geometries because of bigger stagnation zone in the cavity. The shock stand-off distance can be observed maximum in flat plate, while minimum in case of concave shape. The shock envelop also can be shrunk and elongate with concave shape geometry among the three geometries studied. Further, particle induced instability pattern has been studied numerically as steady state and compared with one of the instability pattern found during the experiments with Schlieren image capturing with high-speed camera.

References

- 1) O. Imamura, T. Watanuki, K. Suzuki, E. Rathakrishnan, "Breathing Blunt Nose for drag reduction at hypersonic speeds," *Journal of Visualization*, Dec. 2008, Vol. 11, No. 4, pp 280.
- 2) Khurana S., Suzuki K., "Application of Breathing Blunt Nose Concept to Lifting Body Configuration," 30th AIAA Applied Aerodynamics Conference, June 2013, AIAA 2012-2659.
- 3) Saravanan S., Jagadeesh G., Reddy K.P.J., "Investigation of Missile-Shaped Body with Forward-facing Cavity at Mach 8," *Journal of Spacecraft and Rockets*, Vol. 46, no. 3, 2009, pp. 571-591.
- 4) Khurana S., Suzuki K., "Application of Aerospikes for Lifting Body Configuration in Hypersonic Flow at Mach 7," 43rd AIAA Fluid Dynamics Conference, June 2013,
- 5) Bala V., Jagadeesh, G., Reddy, K.P.J., "Counter-flow drag reduction by supersonic jet for a blunt body in hypersonic flow. *Phys. Fluids*, 2006, 18, 118104
- 6) Myrabo L.N., Raizer Y.P., "Laser-Induced Air Spike for Advanced Transatmospheric Vehicles," 25th AIAA Plasmadynamics and Laser Conference, June 1994, AIAA 94-2451
- 7) Sharma H., Vashishtha A., Rathakrishnan E., "Twin Vortex Flow Physics," *Proceedings of the Institution of Mechanical Engineers, Part G: Journal of Aerospace Engineering*, June, 2008 vol. 222, no. 6, pp. 783-788.
- 8) Arai N., O-Yabu Keishi, "Unsteady flow field around a freely oscillating concave body in supersonic flow," 17th AIAA Aerodynamic Decelerator Systems Technology Conference and Seminar, May 2003, AIAA 2003-2148.
- 9) Mizukaki T., Kawamura N., "Instability Characteristics of Shock Waves ahead of a Hemispherical Shell at Supersonic Speeds," 28th Congress of the International Council of the Aeronautical Sciences, September 2012, ICAS 2012-11.4.2
- 10) Imamura, O., Watanuki, T., Suzuki, K. and Kashiwa Wind Tunnel Working Group (Univ. of Tokyo): "Flow characteristics of UT-Kashiwa Hypersonic Wind Tunnel," *Proceedings of 39th Fluid Dynamics Conference / Aerospace, Numerical Simulation Symposium 2007*, JAXA-SP-07-016, p50-55.
- 11) Yee, H.C., "A class of High-Resolution Explicit and Implicit Shock-Capturing Methods," NASA TM 101088, 1989.
- 12) Shu, C.W., Osher S., "Efficient Implementation of Essentially Non-Oscillatory Shock-Capturing Schemes," *Journal of Computational Physics*, 1988, Vol. 77, pp. 439-471.